An Interpretation of Vibration Tests on Roads By the Impedance Method

M. E. SZENDREI and S. H. KÜHN
Respectively, Senior and Chief Research Officers, National Institute for Road Research, South African Council for Scientific and Industrial Research, Pretoria, Republic of South Africa

A description is given of newly developed light equipment for vibration testing of road constructions. Sinusoidal loading is produced by means of an electrodynamic vibrator exerting vertical forces on the surface of the road or layer under test. The equipment, mounted on a special trailer, is extremely flexible for application to this type of test and permits reliable results to be obtained under a wide variety of conditions.

Two types of test have been carried out: in the impedance method, the ratio of force to resultant velocity is measured in amplitude and phase; in the wave propagation method, wavelengths along the surface are determined. Tests are carried out over a frequency range from 10 c/s to 500 c/s in the impedance method and up to 1,000 c/s in the wave propagation method.

Measurements have been carried out on an experimental road in which widely varying types of construction had been included. From the impedance measurements it was possible to ascribe dynamic parameters to each layer of the construction and, from these, stresses at various depths; and energy losses in the various layers have been calculated.

The potentialities of vibration testing in the control, design and evaluation of road constructions are briefly reviewed.

•THE impedance method of vibration testing of roads, in which an oscillatory force is applied to the road surface and the resultant velocity measured in amplitude and phase is, in principle, a powerful method of investigation in that complete information is gained at any frequency for which measurements are available. Unfortunately no exact theory has been developed up to the present time, because the problem is one of three-dimensional wave propagation in a layered construction, which has defied all attempts at exact mathematical treatment. Even if a mathematical solution were found at some future date, it must of necessity involve a large number of parameters (elastic moduli for each of the layers, thicknesses, etc.) and be of such a form as to render it of little value in its application to practical measurements.

In the present work an attempt has been made to interpret impedance measurements in a manner suggested by the experimental results themselves. With some assumptions and approximations, it is possible to suggest a model of certain elastic properties and geometric dimensions, and from it to estimate certain mechanical quantities which can be related to road performance. The model and all deductions therefrom are put forward as a tentative method of interpreting experimental data. Possibly this approach may lead more speedily to the designing of dynamic tests of practical value to the road engineer.

PRINCIPLE OF IMPEDANCE METHOD

The test consists of applying a vertical force to the surface and measuring both this force and the resultant velocity of the surface in amplitude and phase.

Paper sponsored by Department of Design.

The mechanical impedance, Z, of the construction under test is defined as the ratio of the force, F, exerted on it, to its resultant velocity, v; thus

$$Z = \frac{F}{v} \tag{1}$$

Z is a complex quantity containing a real part, R, and an imaginary part, X, the resistance and reactance, respectively, in which

$$Z = R + jX \tag{2}$$

and $j = \sqrt{-1}$.

Unless the system contains internal sources of mechanical energy, R must be positive; the reactance, X, may be positive or negative.

If θ is the phase angle defined by

$$\theta = \tan^{-1} \frac{X}{R} \tag{3}$$

and $|Z|$ is the amplitude of Z, the following relations hold:

$$|Z| \cos\theta = R \tag{4}$$

$$|Z| \sin\theta = X \tag{5}$$

$$Z^2 = R^2 + X^2 \tag{6}$$

Experimentally the R M S amplitudes of F and v are measured, so that $|Z|$ is calculated directly from Eq. 1. The phase angle, θ, is also measured, and the quantities R and X become then immediately available from Eqs. 4 and 5 at any frequency for which the measurements have been taken.

EQUIPMENT USED IN THE TESTS

Sinusoidal vertical forces are produced by an electrodynamic force generator bolted to the lower face of a cast iron cylinder weighing one ton. During tests, the cylinder is supported by two reinforced motorcycle innertubes fitting around its circumference and resting on circular brackets. The cylinder and its supports are mounted on a mo-

Figure 1. Station wagon and trailer set up for an impedance test.

bile trailer suspension system. An International station wagon is used to tow the trailer and house the associated electronic equipment. Figure 1 shows the station wagon and trailer set up for an impedance test.

Details of the equipment used for applying forces to the road surface are shown diagrammatically in Figure 2. Exhaustive tests have indicated that, in its present form, the equipment is suitable for impedance measurements covering the range from 10 c/s to 500 c/s. Although the forces generated are relatively low (not greater than 20 lb), they are sufficient to produce measurable velocities well above the background noises. Such forces can probably provide all the information obtainable from the application of larger forces, as road constructions have been found to be linearly elastic for forces up to 2 tons (1).

The electronic equipment is shown diagrammatically in Figure 3. It should be noted that both geophone and preamplifier must be calibrated for amplitude and phase over the whole frequency range to be investigated. The force output from the vibrator is monitored on the ammeter.

Experimental results for a particular site are most conveniently presented as two

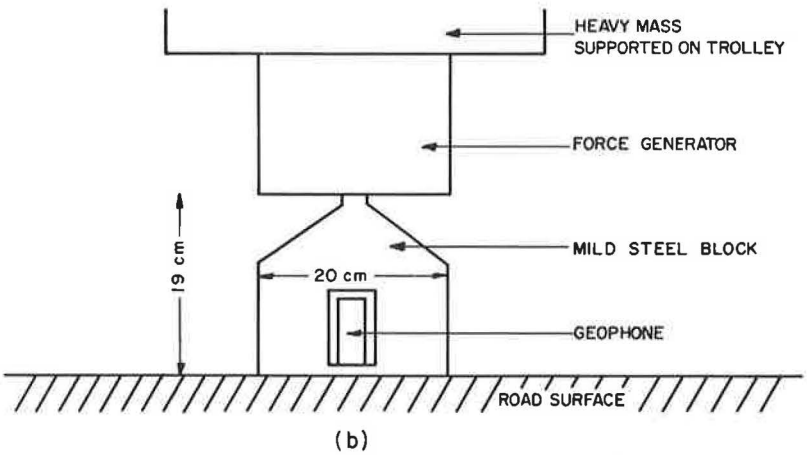

Figure 2. Framework through which forces are applied to surface.

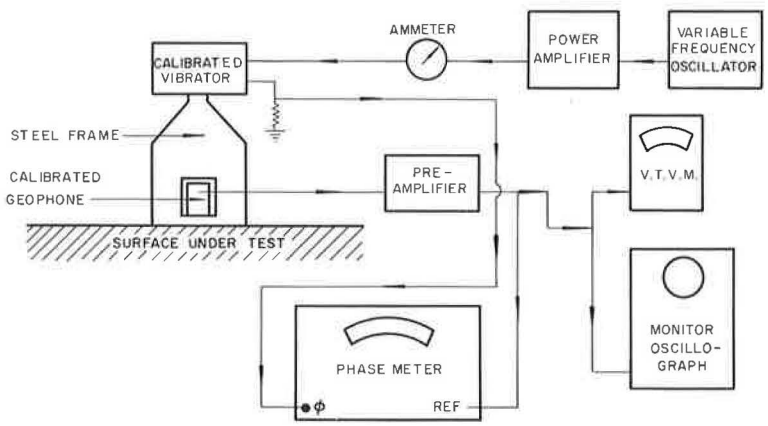

Figure 3. Block diagram of electronic equipment.

graphs relating X and R as functions of frequency. Typical curves are shown in Figures 4 and 5. It should be remarked that, except near resonance, ωX is numerically much larger than R and the phase angle, θ, is large; it therefore follows from Eqs. 4 and 5 that X can be determined more accurately than R.

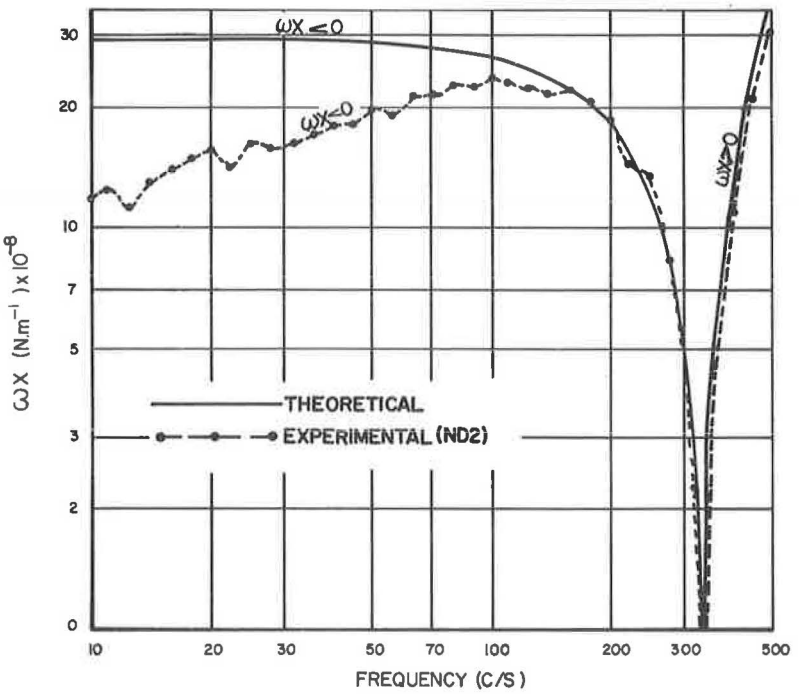

Figure 4. Typical ωX against frequency curve.

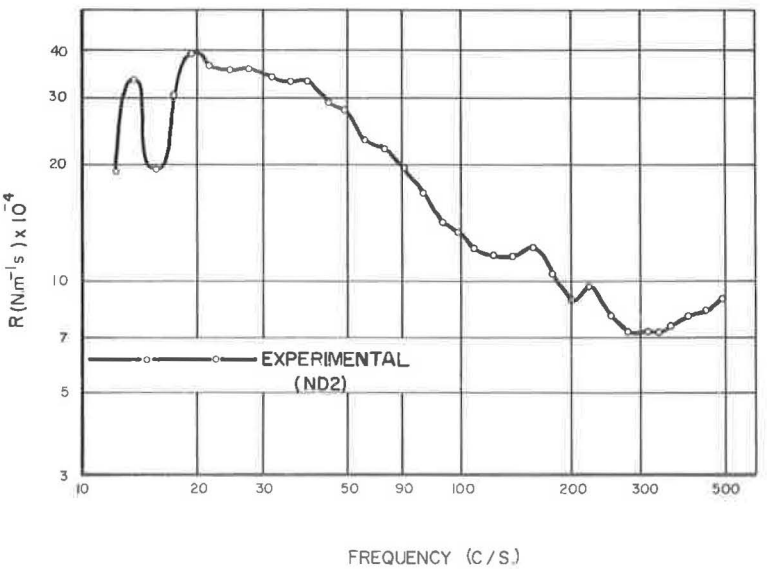

Figure 5. Typical R vs frequency curve.

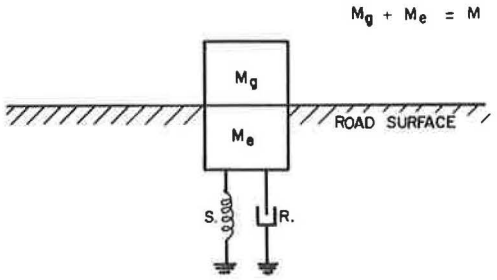

Figure 6. Assumed three-parameter model.

INTERPRETATION OF DATA FROM A MODEL WITH THREE CONSTANT PARAMETERS

The simplest mechanical model, for which the ωX function approximates in shape to the corresponding experimental curve, consists of a fixed M restrained in its motion by a spring of stiffness, S, and a frictional resistance, R (Fig. 6).

For this model the mechanical impedance, Z, offered to an impressed oscillatory force of frequency, f, is given by (2)

$$Z = R + j\left(\omega M - \frac{S}{\omega}\right) \qquad (7)$$

in which $\omega = 2\pi f$.

Identifying Eqs. 2 and 7, it follows immediately that: (a) the resistance, R, of Eq. 7 corresponds to the real part R of Eq. 2; and (b) the reactance, X, of Eq. 2 is related to the mass, M, and stiffness, S, of the adopted model by the relation:

$$X = \omega M - \frac{S}{\omega} \qquad (8)$$

or

$$\omega X = \omega^2 M - S \qquad (9)$$

A comparison between an experimental ωX curve and the corresponding theoretical curve obtained from Eq. 9 is shown in Figure 4, where the values of M and S for the theoretical curve were deduced from the experimental points around resonance (in which $\omega X \approx 0$).

The curves agree fairly well at higher frequencies, thus justifying the assumption of the three-parameter model. The greatest discrepancy occurs at low frequencies where the experimental curve is numerically lower than the theoretical one. The difference cannot be ignored, particularly as it occurs at all sites where the construction is of reasonably high quality. Furthermore, the R curve (Fig. 5), which should be constant with frequency, shows an appreciable drop. Hence it must be concluded that the parameters are not constant over the whole frequency range investigated, and the model with three frequency independent parameters is inadequate.

MORE COMPLETE INTERPRETATION OF EXPERIMENTAL DATA

It was suggested by Lorenz (3) that, for a three-parameter model of constant coefficients, ωX be plotted as a function of the square of the frequency, where a straight line should result; by putting $y = \omega X$ and $x = f^2$, Eq. 9 becomes

$$y = (4\pi^2 M)\, x - S \qquad (10)$$

The intercept on the y-axis is thus equal to -S and the gradient to $4\pi^2 M$; both M and S can therefore be determined, if these parameters are independent of frequency. Heukelom (4) in Holland and Baum (5) in Germany have adopted this approach and obtained some interesting results. Baum in particular, whose equipment operates between 10 and 70 c/s, has found that a plot of ωX vs f^2 falls along two straight lines, indicating two effective models each with its own constant parameters.

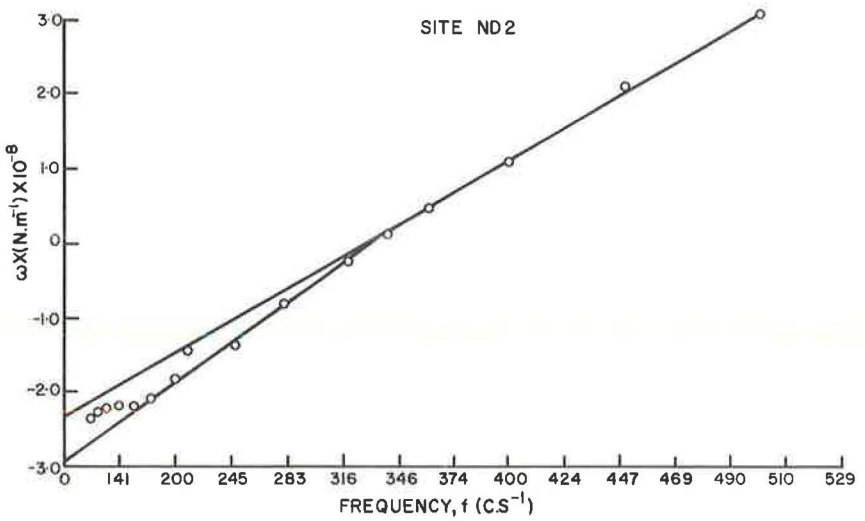

Figure 7. Plot of ωX vs f^2 for site ND2—high frequency range.

When this method is applied to measurements made by the authors it is found that, depending on the type of construction, one or two straight lines are obtained over the higher frequency range (Fig. 7) and sometimes even three lines. From this information the results given in Table 1 were compiled on the assumption that, in the frequency range where a number of successive experimental points lie on a straight line, the values of M and S are constant. According to Eq. 10 this is valid, unless S and M both vary in such a way that the variation of one exactly compensates for the variation of the other, which is most unlikely.

Straight lines on the ωX vs f^2 plot are obtained at the higher frequencies, usually above 100 c/s, depending on the type of construction. The fact that no use is made of the low frequency measurements is unsatisfactory in that some useful information must be contained in the data below 100 c/s.

In preliminary work it had been noted that, if S were assumed constant at low frequencies and equal in value to that obtained from the ωX vs f^2 straight lines, the experimental points followed quite well the theoretical values for M, obtained on the assumption that it varied according to

$$M = B f^{\alpha} \tag{11}$$

B and α being constants. B represents the mass when $f = 1$ and α was found to lie between -2 and -3. Experimental data therefore had indicated a very rapid increase in mass with decrease in frequency over the lower frequency range.

Physical considerations would also suggest a value of $\alpha = -3$, because, in a uniform medium with the wave velocity constant, the wave length, λ, is inversely proportional to the frequency.

$$\lambda \propto f^{-1} \tag{12}$$

Whatever the shape of the effective volume of disturbed material, its dimensions should be proportional to the wave length, and the volume to λ^3 or f^{-3}. Hence, the mass, M, would also be expected to vary as f^{-3}.

TABLE 1

VALUES OF S, M AND R DEDUCED FROM DATA SHOWN IN FIGURES 4 AND 5

Frequency (c/s)	S(N m^{-1})	M (kg)	R(N m^{-1}s)
100 - 140	2.54×10^6	506	1.20×10^5
160 - 320	2.95×10^6	67	8.97×10^4
340 - 500	2.43×10^6	56	7.88×10^4

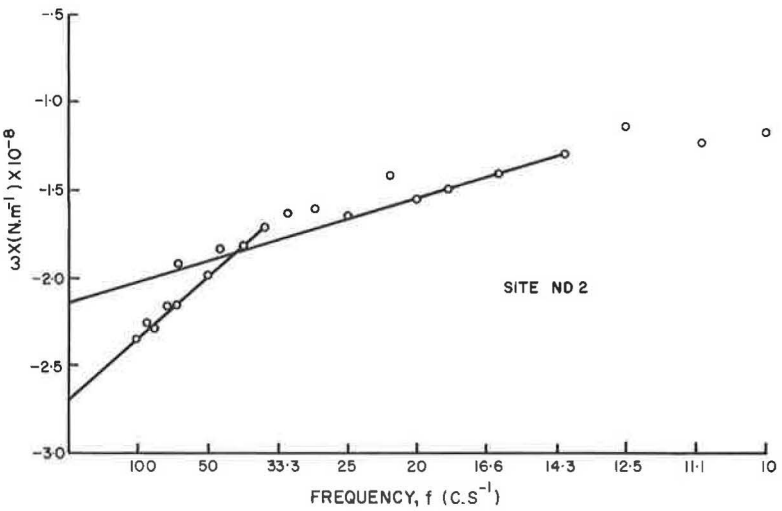

Figure 8. Plot of ωX vs f^{-1} for site ND2—low frequency range.

Therefore, it was assumed that the mass is given by

$$M = \pi B f^{-3} \tag{13}$$

Substituting Eq. 13 in Eq. 9 gives

$$X = (4\pi^2 B) f^{-1} - S \tag{14}$$

A plot of ωX vs $1/f$ should therefore give a straight line in a region where S is constant and M varies according to Eq. 13. Figure 8 shows a plot of ωX vs $1/f$ for one of the sites tested. Two straight lines could be drawn through the experimental points, from each of which values of S and B have been obtained (Table 2).

Using both the f^2 and f^{-1} plots it seems possible to classify the dynamic behavior of a road construction into a number of frequency ranges each having appropriate S and M values. Whereas the value of S is always constant in a given range, the value of M is only constant where its value is obtained from the f^2 plot. If the B-value is deduced from the ωX vs f^{-1} plot, the correct value of M at any frequency within the range of validity must be obtained from Eq. 13.

In view of the relatively larger scatter of the experimental points in Figure 5, a mean value of R for the frequency range, defined by the ωX straight-line relationships (Figs. 7 and 8), has been assumed. Values of R for site ND2 are given in the last columns of Tables 1 and 2.

DESCRIPTION OF EXPERIMENTAL SITES AND DATA

The measurements described here were made along an experimental length (approximately 1 mile) at Key Ridge on the southbound roadway of route N3/1 between Durban and Pietermaritzburg in Natal. The experimental length consists of 24 sections, each 200 ft long, and of different types of construction. Only 14

TABLE 2

VALUES OF S, B AND R OBTAINED FROM FIGURES 5 AND 2

Frequency (c/s)	S (N m^{-1})	B (kg s^{-3})	R (N m^{-1} s)
14 - 20	2.16×10^8	3.04×10^7	3.05×10^5
36 - 100	2.70×10^8	8.99×10^7	2.31×10^5

TABLE 3

EXPERIMENTAL VALUES OF THREE PARAMETERS FOR EACH FREQUENCY RANGE OBTAINED AT EACH POSITION OF SITE ND13

Position	1	2	3	Mean
Freq. range (c/s)	320 - 500	250 - 500	200 - 400	257 - 467
S(N m^{-1})	2.65 × 10^8	2.47 × 10^8	2.10 × 10^9	2.41 × 10^8
M (kg)	39	34.7	32.9	35.5
R (N m^{-1}s)	1.24 × 10^5	1.11 × 10^5	1.03 × 10^5	1.13 × 10^5
Freq. range (c/s)	80 - 125	80 - 160	80 - 200	80 - 162
S (N m^{-1})	2.46 × 10^8	2.08 × 10^8	1.82 × 10^8	2.12 × 10^8
B (kg s^{-3})	1.72 × 10^6	1.29 × 10^8	1.24 × 10^8	1.42 × 10^8
R (N m^{-1}s)	2.49 × 10^5	2.28 × 10^5	1.69 × 10^5	2.15 × 10^5
Freq. range (c/s)	45 - 64	50 - 71	40 - 71	45 - 69
S (N m^{-1})	1.89 × 10^8	1.66 × 10^8	1.30 × 10^8	1.62 × 10^8
B (kg s^{-3})	6.45 × 10^7	5.44 × 10^7	2.53 × 10^7	4.81 × 10^7
R (N m^{-1}s)	3.15 × 10^5	2.73 × 10^5	2.20 × 10^5	2.69 × 10^5
Freq. range (c/s)	20 - 28	16 - 40	10 - 40	15 - 36
S (N m^{-1})	1.41 × 10^8	1.31 × 10^8	1.12 × 10^8	1.28 × 10^8
B (kg s^{-3})	1.34 × 10^7	1.11 × 10^7	7.59 × 10^6	1.07 × 10^7
R (N m^{-1}s)	3.43 × 10^5	2.90 × 10^5	2.81 × 10^5	3.05 × 10^5

of the 24 sections were tested, profiles of which are shown schematically in Figures 9 through 12. All measurements were taken at a distance of 6 ft from the edge of the surfacing and three impedance tests were carried out on each section at 6-ft intervals. On section ND2, only one impedance test was made because of the steep gradient.

The data obtained on the various sites were analyzed as outlined in the previous section. Good agreement was found in regard to the number of straight lines for the three positions of each test site. A fair degree of variation was found in the parameters determined from the three sets of measurements taken on each section (Table 3). The mean values of the parameters obtained at the three sites on each section are given in Tables 4 to 7 in which the experimental sites have been grouped according to the type of construction, as follows: (a) group 1 (Fig. 9)—sites with various thicknesses of surfacing over "in-place" material; it should be noted that all these sites occurred in "cut," where the

TABLE 4

VALUES OF S OBTAINED BY THE METHOD FROM A MODEL WITH THREE CONSTANT PARAMETERS

Experimental Site	Frequency Range No. 1		Frequency Range No. 2		Frequency Range No. 3		Frequency Range No. 4		Frequency Range No. 5	
	Frequency (c/s)	S (N m^{-1})	Frequency (c/s)	S (N m^{-1})	Frequency (c/s)	S (N m^{-1})	Frequency (c/s)	S (N m^{-1})	Frequency (c/s)	S (N m^{-1})
ND5	10 - 23	1.36 × 10^8	27 - 67	1.73 × 10^8	160 - 310	2.07 × 10^8	333 - 500	1.53 × 10^8	-	-
ND8	83 - 147	1.01 × 10^8	273 - 450	8.50 × 10^7	-	-	-	-	-	-
ND9	17 - 35	1.35 × 10^8	107 - 200	1.38 × 10^8	333 - 500	6.67 × 10^7	-	-	-	-
ND10	10 - 32	1.35 × 10^8	28 - 53	1.38 × 10^8	120 - 200	1.55 × 10^8	320 - 500	1.41 × 10^8	-	-
ND15	15 - 47	1.17 × 10^8	64 - 97	1.57 × 10^8	247 - 500	1.90 × 10^8	-	-	-	-
ND2	14 - 20	2.16 × 10^8	36 - 100	2.70 × 10^8	100 - 140	2.54 × 10^8	160 - 320	2.95 × 10^8	340 - 500	2.43 × 10^8
ND6	10 - 16	1.28 × 10^8	20 - 40	1.54 × 10^8	51 - 97	2.13 × 10^8	220 - 303	2.27 × 10^8	347 - 500	2.11 × 10^8
ND7	15 - 39	2.36 × 10^8	68 - 140	3.83 × 10^8	347 - 483	4.52 × 10^8	-	-	-	-
ND11	16 - 45	1.64 × 10^8	65 - 173	2.80 × 10^8	333 - 500	3.48 × 10^8	-	-	-	-
ND12	17 - 38	1.79 × 10^8	44 - 93	2.16 × 10^8	167 - 287	2.45 × 10^8	340 - 500	2.40 × 10^8	-	-
ND3	29 - 42	3.66 × 10^8	50 - 113	3.61 × 10^8	180 - 265	7.25 × 10^8	280 - 385	4.06 × 10^8	410 - 500	2.70 × 10^8
ND4	17 - 27	3.83 × 10^8	42 - 64	5.40 × 10^8	66 - 110	7.50 × 10^8	147 - 297	1.07 × 10^9	353 - 460	2.50 × 10^8
ND13	15 - 36	1.28 × 10^8	45 - 69	1.62 × 10^8	80 - 162	2.12 × 10^8	257 - 467	2.41 × 10^8	420 - 500	1.65 × 10^8
ND14	13 - 37	1.77 × 10^8	45 - 128	2.75 × 10^8	180 - 260	3.26 × 10^8	-	-	-	-

TABLE 5

VALUES OF R OBTAINED BY THE METHOD FROM A MODEL WITH THREE CONSTANT PARAMETERS

Experimental Site	Frequency Range No. 1		Frequency Range No. 2		Frequency Range No. 3		Frequency Range No. 4		Frequency Range No. 5	
	Frequency (c/s)	R (N m^{-1}s)	Frequency (c/s)	R (N m^{-1}s)	Frequency (c/s)	R (N m^{-1}s)	Frequency (c/s)	R (N m^{-1}s)	Frequency (c/s)	R (N m^{-1}s)
ND5	10 - 23	2.82 × 10^5	27 - 67	2.45 × 10^5	160 - 310	9.60 × 10^4	333 - 500	9.01 × 10^4	-	-
ND8	83 - 147	3.37 × 10^5	273 - 450	2.94 × 10^5	-	-	-	-	-	-
ND9	17 - 35	2.03 × 10^5	107 - 200	1.35 × 10^5	333 - 500	1.25 × 10^5	-	-	-	-
ND10	10 - 32	3.12 × 10^5	28 - 53	2.41 × 10^5	120 - 200	1.66 × 10^5	320 - 500	1.52 × 10^5	-	-
ND15	15 - 47	2.23 × 10^5	67 - 97	1.67 × 10^5	247 - 500	7.60 × 10^4	-	-	-	-
ND2	14 - 20	3.05 × 10^5	36 - 100	2.31 × 10^5	100 - 140	1.20 × 10^5	160 - 320	8.97 × 10^4	340 - 500	7.88 × 10^4
ND6	10 - 16	3.10 × 10^5	20 - 40	2.94 × 10^5	51 - 97	1.91 × 10^5	220 - 303	6.21 × 10^4	347 - 500	3.23 × 10^4
ND7	15 - 39	4.69 × 10^5	68 - 140	3.11 × 10^5	347 - 483	8.93 × 10^4	-	-	-	-
ND11	16 - 45	3.30 × 10^5	65 - 173	2.32 × 10^5	333 - 500	6.52 × 10^4	-	-	-	-
ND12	17 - 36	3.33 × 10^5	44 - 93	1.69 × 10^5	167 - 287	7.46 × 10^4	340 - 500	5.06 × 10^4	-	-
ND3	29 - 42	6.45 × 10^5	50 - 113	4.57 × 10^5	180 - 265	4.46 × 10^5	280 - 385	1.54 × 10^5	410 - 500	1.56 × 10^5
ND4	17 - 27	1.03 × 10^6	42 - 64	1.11 × 10^6	66 - 110	1.08 × 10^6	147 - 297	9.14 × 10^5	353 - 460	7.76 × 10^5
ND13	15 - 36	3.05 × 10^5	45 - 69	2.69 × 10^5	80 - 162	2.15 × 10^5	257 - 467	1.13 × 10^5	420 - 500	8.09 × 10^4
ND14	13 - 37	4.34 × 10^5	45 - 128	3.12 × 10^5	180 - 260	1.73 × 10^5	-	-	-	-

TABLE 6

VALUES OF B OBTAINED BY THE METHOD FROM A MODEL WITH THREE CONSTANT PARAMETERS

Experimental Site	Frequency Range No. 1		Frequency Range No. 2		Frequency Range No. 3		Frequency Range No. 4		Frequency Range No. 5	
	Frequency (c/s)	B ($kg\ s^{-3}$)	Frequency (c/s)	B ($kg\ s^{-3}$)	Frequency (c/s)	B ($kg\ s^{-3}$)	Frequency (c/s)	B ($kg\ s^{-3}$)	Frequency (c/s)	B ($kg\ s^{-3}$)
ND5	18 - 23	1.01×10^7	27 - 67	3.60×10^7	-	-	-	-	-	-
ND8	-	-	-	-	-	-	-	-	-	-
ND9	17 - 35	1.93×10^7	-	-	-	-	-	-	-	-
ND10	10 - 32	1.57×10^7	28 - 53	2.36×10^7	-	-	-	-	-	-
ND15	15 - 47	8.86×10^6	64 - 97	6.08×10^7	-	-	-	-	-	-
ND2	14 - 20	3.04×10^7	36 - 100	8.99×10^7	-	-	-	-	-	-
ND6	10 - 16	6.16×10^6	20 - 40	1.20×10^7	51 - 97	7.56×10^7	-	-	-	-
ND7	15 - 39	2.06×10^7	68 - 140	2.32×10^8	-	-	-	-	-	-
ND11	16 - 45	2.86×10^7	65 - 173	1.93×10^8	-	-	-	-	-	-
ND12	17 - 36	2.00×10^7	44 - 93	5.53×10^7	-	-	-	-	-	-
ND3	29 - 42	1.34×10^8	50 - 113	1.55×10^8	180 - 265	1.58×10^9	-	-	-	-
ND4	17 - 27	4.94×10^7	42 - 64	2.52×10^8	66 - 110	6.14×10^8	147 - 297	2.21×10^9	353 - 460	1.44×10^{10}
ND13	15 - 36	1.07×10^7	45 - 69	4.81×10^7	80 - 162	1.42×10^8	-	-	-	-
ND14	13 - 37	1.31×10^7	45 - 128	1.18×10^8	-	-	-	-	-	-

TABLE 7

VALUES OF M OBTAINED BY THE METHOD FROM A MODEL WITH THREE CONSTANT PARAMETERS

Experimental Site	Frequency Range No. 3		Frequency Range No. 4		Frequency Range No. 5	
	Frequency (c/s)	M (kg)	Frequency (c/s)	M (kg)	Frequency (c/s)	M (kg)
ND5	160 - 310	56.1	333 - 500	44.8	-	-
ND8	83 - 147	37.0	273 - 450	32.0	-	-
ND9	107 - 200	58.8	333 - 500	50.4	-	-
ND10	120 - 200	70.4	320 - 500	62.6	-	-
ND15	247 - 500	39.6	-	-	-	-
ND2	100 - 140	506	160 - 320	67.0	340 - 500	56.0
ND6	220 - 303	43.2	347 - 500	42.5	-	-
ND7	347 - 483	43.1	-	-	-	-
ND11	333 - 500	53.1	-	-	-	-
ND12	167 - 287	54.4	340 - 500	51.2	-	-
ND3	280 - 385	63.3	410 - 500	41.7	-	-
ND4	-	-	-	-	-	-
ND13	257 - 467	35.5	420 - 500	27.8	-	-
ND14	180 - 260	63.9	-	-	-	-

foundation might be expected to be above average strength; (b) group 2 (Fig. 10)—sites with foundation composed of base, subbase and subgrade, none of them stabilized; (c) group 3 (Fig. 11)—sites with a stabilized subbase; and (d) group 4 (Fig. 12)—sites with stabilized bases. All the sites of groups 2, 3 and 4 are on varying amounts of fill.

The total number of straight lines which could be found varies from a minimum of 2 to a maximum of 5; there also seems to be a slight tendency for this number to increase for constructions with stabilization either in the subbase or base.

The value of S always increases with frequency up to a broad maximum in the highest or second highest frequency range. On the other hand, R, decreases at various rates as the frequency increases.

From Eq. 13 and the values of B given in Table 6, it is seen that the decrease in M with increase in f is very rapid at low frequencies. At the high frequencies the mass remains constant over considerable ranges of frequency; however, the mass still decreases with increase in frequency in a number of steps.

The total mass, M, consists of the effective ground mass, M_e, which takes part in the vibration, and the mass, M_g, of the equipment below the force generator which also vibrates rigidly (Fig. 6). With the present equipment M_g = 34 kg, so that M can never be smaller than this value. Although the values of M obtainable from Table 6 over the low frequences are clearly much greater than this critical value, this condition is also

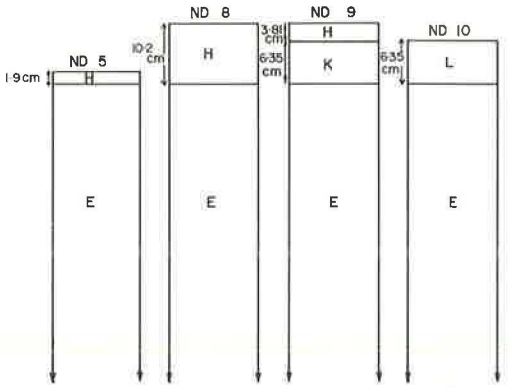

H = BRITISH STANDARD 594 - HOT ROLLED ASPHALT

E = INPLACE MATERIAL

K = CRUSHER RUN BASECOURSE

L = PENETRATION MACADAM

Figure 9. Profiles of test sites consisting of surfacing only.

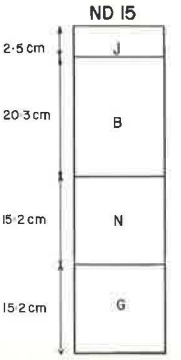

J = 2 COAT SURFACE TREATMENT

B = REPLACED CRUSHER RUN BASECOURSE COMPACTED TO ≮ 98% MAASHO

N = NEW SUBBASE MATERIAL EX KEY RIDGE CUT COMPACTED TO ≮ 95% MAASHO

G = MINIMUM INPLACE DENSITY 95% MAASHO

Figure 10. Profile of test site with unstabilized foundation.

satisfied in all cases shown in Table 7 except two (the second value for ND8 and the second value for ND13), where M is slightly smaller than 34 kg. The tendency of M towards this independently measured critical value confirms, therefore, the following points: (a) the part of the equipment below the force generator may indeed be considered rigid up to 500 c/s; (b) the calibration of all transducers and electronic equipment is sound; and (c) the measurements are, on the whole, reliable and have been correctly reduced up to this stage.

Although no mean values of M for each site can be taken on account of its rapid variation with frequency, some significance could be attached to the mean value of the other two parameters (S and R), as their variation with frequency is much smaller. The mean values of S and R for each site and each group are given in Table 8.

Considering the mean values for each group, it is noted that S is lowest for group 1 and highest for group 4. Group 4 also shows the largest value of R, while the lowest value occurs for group 2. However, there are considerable differences between the site values within each group, a fact not altogether surprising because the grouping was done in a rather arbitrary way as regards amount and type of stabilization. The high values for site ND4, which are presumably related to the 6 percent cement stabilization of the base, and the relatively low values for site ND13 where the base is stabilized with lime instead of cement, should be noted.

The differences between the means of each group are not much greater than the scatter within each group and therefore nothing further of significance can be deduced.

The stiffnesses, S, in Table 8 were compared with a few Benkelman beam results carried out on the same sites. An inverse correlation was noted between the stiffnesses found from impedance measurements and the deflections from the Benkelman beam tests, high values of S being usually associated with small deflections.

WAVE PROPAGATION TESTS

Another form of vibration testing makes use of the wave propagation method, in which the wave lengths of vertical surface waves are determined for various frequencies. The data are usually presented on a phase velocity vs wave length plot (Fig. 13) and interpreted in terms of a theory developed by Jones (6). For a layered construction, the dispersion graph results in a number of branches from which the sheer moduli and thicknesses of the layers can be determined accurately.

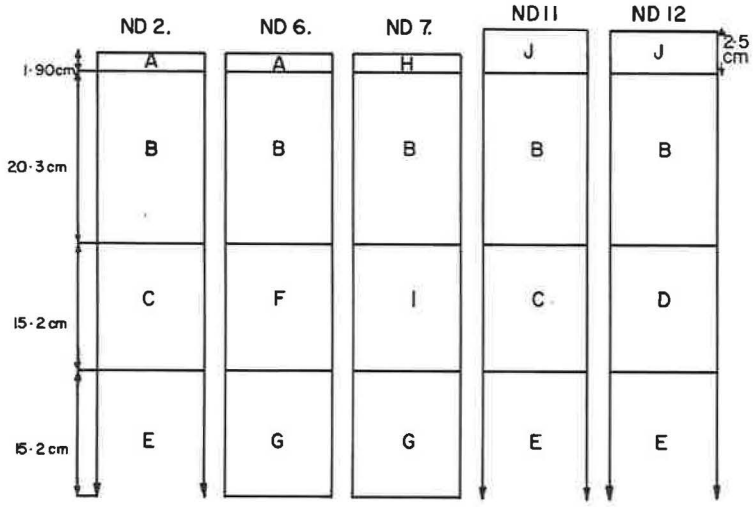

A = FLEXIBLE PREMIX.

B = REPLACED CRUSHER RUN BASECOURSE COMPACTED TO ≮ 98% MAASHO.

C = INPLACE MATERIAL COMPACTED TO ≮ 95% MAASHO AND STABILISED WITH 4% CEMENT.

D = INPLACE MATERIAL COMPACTED TO ≮ 95% MAASHO AND STABILISED WITH 6% MARVELLO WHITE ROAD LIME.

E = INPLACE MATERIAL.

F = NEW SUBBASE MATERIAL EX KEY RIDGE CUT COMPACTED TO ≮ 95% MAASHO STABILISED WITH 6% CEMENT.

G = MINIMUM INPLACE DENSITY 95% MAASHO.

H = BRITISH STANDARD 594 — HOT ROLLED ASPHALT.

I = NEW SUBBASE MATERIAL EX KEY RIDGE CUT COMPACTED TO ≮ 95% MAASHO STABILISED WITH 4% CEMENT.

J = 2 COAT SURFACE TREATMENT.

Figure 11. Profiles of test sites with stabilized subbase.

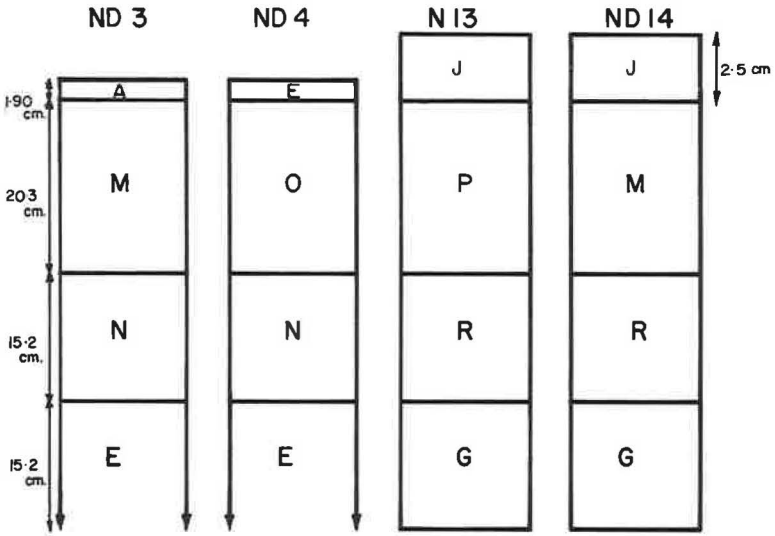

A = FLEXIBLE PREMIX.

M = REPLACED CRUSHER RUN BASECOURSE COMPACTED TO ≮ 98% MAASHO STABILISED WITH 4% CEMENT.

N = NEW SUBBASE MATERIAL EX KEY RIDGE CUT COMPACTED TO ≮ 95 % MAASHO.

E = INPLACE MATERIAL.

H = BRITISH STANDARD 594 - HOT ROLLED ASPHALT.

O = REPLACED CRUSHER RUN BASECOURSE COMPACTED TO ≮ 98% MAASHO STABILISED WITH 6% CEMENT.

J = 2 COAT SURFACE TREATMENT.

P = REPLACED CRUSHER RUN BASECOURSE COMPACTED TO ≮ 98% MAASHO STABILISED WITH 6% MARVELLO WHITE ROAD LIME.

R = INPLACE MATERIAL COMPACTED TO ≮ 95% MAASHO.

G = MINIMUM INPLACE DENSITY 95% MAASHO.

Figure 12. Profiles of test sites with stabilized base.

TABLE 8

MEAN VALUES OF S AND R FOR EACH SITE AND FOR EACH GROUP

Group	Site	S (N m^{-1})	R (N m^{-1} s)
1	ND5	1.54×10^8	1.81×10^5
	ND8	9.30×10^7	3.15×10^5
	ND9	1.13×10^8	1.54×10^5
	ND10	1.38×10^8	2.18×10^5
	Mean	1.24×10^8	2.17×10^5
2	ND15	1.53×10^8	1.55×10^5
3	ND2	2.56×10^8	1.65×10^5
	ND6	1.87×10^8	1.78×10^5
	ND7	3.57×10^8	2.90×10^5
	ND11	2.64×10^8	2.09×10^5
	ND12	2.20×10^8	1.57×10^5
	Mean	2.57×10^8	2.00×10^5
4	ND3	4.26×10^8	3.72×10^5
	ND4	1.05×10^9	9.82×10^5
	ND13	1.82×10^8	1.97×10^5
	ND14	2.59×10^8	3.06×10^5
	Mean	4.79×10^8	4.64×10^5

Wave propagation tests were carried out on all the sites where impedance measurements had been made. The exciting forces were produced with the same equipment (vibration generator mounted under the trailer). Wave lengths were determined by measuring the increase in phase angle with increasing distance at various frequencies. The equipment was, unfortunately, unsuitable for measurements much above 1,000 c/s, with the result that: (a) the shear moduli of the surfacing could not be determined; (b) the shear moduli of the base course could only be determined approximately; and (c) thicknesses of the layers could not be calculated exactly from the measurements, but had to be estimated by assuming that the depth at which the elastic constants were determined was one-third of the wave length.

Profiles of the type shown in Figure 14 were calculated from the results obtained by this method and it was found that, in spite of the approximate method of determining depths, there was no difficulty in identifying the layers to which the shear moduli referred.

The thicknesses, although approximate, were used in later calculations to determine the geometry of the vibrating mass in the subbase and subgrade, where they were not always given in the design profile.

GEOMETRICAL SHAPE OF VIBRATING MASS

Values of the three parameters (mass, stiffness and resistance) cannot easily be related to the mechanical properties of road foundations with which the engineer is

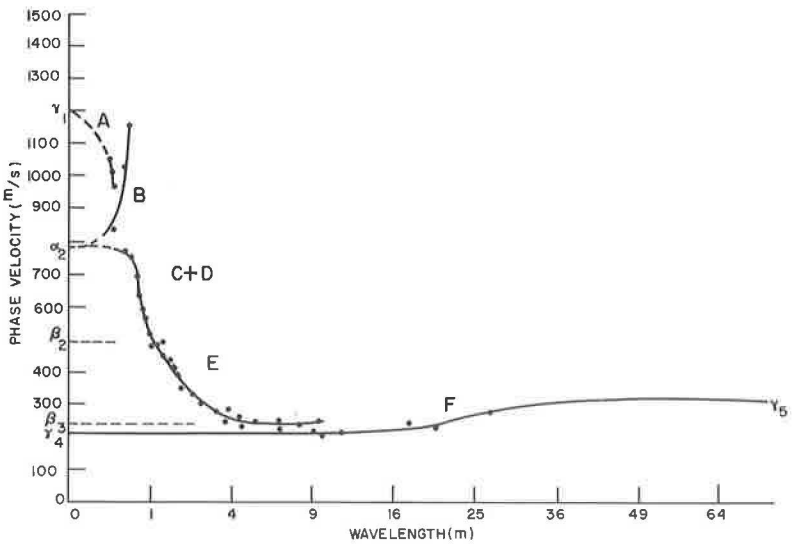

Figure 13. Phase velocity vs wave length graph for site ND 3.

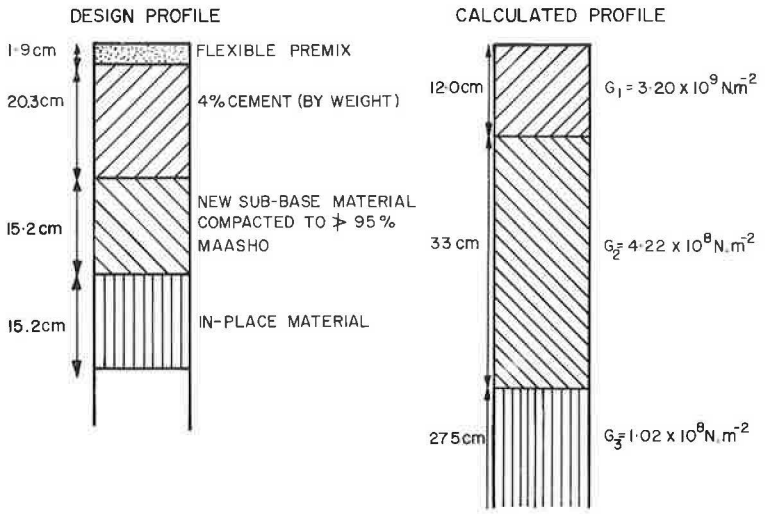

Figure 14. Design and calculated profiles for site ND 3.

familiar. On the other hand, impedance measurements are reasonably accurate and repeatable and, from their nature, should be usefully related to the mechanical properties of the constructions under test. The method of working with averaged values of S and R may give an overall picture of the construction, but what is required is more detailed information on the mechanical properties of each layer of the construction which would offer some indication of whether under-design or over-design has occurred.

More rational use must therefore be made of the measurements and their variation with frequency and, because of the lack of an adequate theory, a geometrical model is postulated which represents an approximation to actual conditions. In so doing the following observations have been borne in mind:

1. The three-parameter model implies a rigid mass of material in a state of vibration, restrained by frictional and elastic forces.
2. The vibrating mass varies rapidly with frequency, but in a somewhat irregular manner. At the higher frequencies it changes in a series of steps, while at the lower frequencies it varies continuously according to an inverse cube law as well as in steps as reflected in sudden changes in B (Eq. 13).
3. The number of steps is of the same order as the number of layers of the construction.
4. Both theory of, and experimental evidence from, the wave propagation method show that lower frequencies penetrate to greater depths of the construction.

These points suggest that a discontinuous increase in mass indicates that an additional layer has attached itself to the vibrating mass. If the layer is thin and bound together by strong internal forces, the transition from one layer to the next is represented by a sudden change in mass, while if the layer is thick and bound by weak internal forces, the increase in mass is continuous within the layer, while transition to a lower layer is accompanied by a change in B. If the thicknesses and densities of the various layers are known, it is possible to build a geometrical model using the variation in M obtained by impedance measurements.

The geometrical shape of the vibrating mass in each layer must be symmetrical in a horizontal plane, and static elastic theories also indicate that the load spreads in area as the depth increases; accordingly a frustum of a cone suggests itself for all the layers except the surfacing. To avoid unreasonably large spreads, which were found to occur for the surfacing, a cylinder has therefore been used to represent the shape of the top mass.

It does not necessarily follow that the number of frequency ranges must always be exactly equal to the number of layers in the road profile. Strong cohesive forces between two layers may give rise to a single frequency range (or M step). If a horizontal crack develops within one layer, or there occurs a horizontal boundary to the composition in a natural soil, the nominally single layer may give rise to more than one frequency range (or M step).

In the present series of measurements, the nominal thicknesses of the top layers were available from the design sheets for the experimental road supplied by the Department of Transport. The use of these values is not entirely satisfactory because the thicknesses of the actual construction may probably differ from those indicated in the design profile. A method based on wave propagation measurements is being developed by which it should be possible to determine thicknesses in situ to a fair degree of accuracy.

In practice, densities normally lie between 90 and 150 pcf and therefore represent a maximum variation of 25 percent about a mean. It will further be shown that a slightly incorrect density does not affect significantly the final results. Accordingly, for the determination of these models, a uniform density of 2×10^3 kg/cu m (equivalent to 120 pcf has been used.

In the following treatment the layers of the construction are numbered progressively from the top downwards, as follows: subscript 1 refers to the surfacing; subscript 2, to the base; subscript 3, to the subbase; subscript 4, to the subgrade. If M is the total mass obtained from the measurements at a given frequency and n layers are affected at that frequency

$$M = M_g + M_1 + \ldots = M_n \tag{15}$$

in which M_g is the apparent mass and $M_1 \ldots M_n$ are the layer masses taking part in the vibration. Because all the M's up to M_{n-1} are known from measurements at higher frequencies, M can be obtained by subtraction. In cases where M is a function of frequency, M has been calculated (Eq. 13) for the lowest frequency in the relevant frequency range. With these conditions in mind the following basic procedure was adopted to determine the geometrical shape of the models for each of the sites (Fig. 18):

1. The radius of the cylindrical mass associated with the surfacing was determined from the experimentally measured mass, M_1, and design height, h_1, from

$$r_1^2 = r_2^2 = \frac{M_1}{\pi h_1 \rho} \tag{16}$$

2. With r_2 determined, M_2 known from impedance measurements, and h_2 obtained from the design profile, a conical shape for the second block was assumed and its radius at the base, r_3, and the vertical angle, θ_2, determined from

$$r_3^2 + r_3 r_2 + r_2^2 = \frac{3 M_2}{\rho \pi h_2} \tag{17}$$

and

$$\tan \theta_2 = \frac{r_3 - r_2}{h_2} \tag{18}$$

3. The vertical angles of the lower blocks were obtained from the ratios of the elastic moduli of adjacent layers as determined from wave propagation experiments, according to

$$\frac{\tan \theta_n}{\tan \theta_{n+1}} = \left[\frac{E_n}{E_{n+1}}\right]^{1/2} = \left[\frac{G_n}{G_{n+1}}\right]^{1/2} \tag{19}$$

in which E_n and G_n are the Young's and shear moduli of the nth layer.

Eq. 19 (which assumes equal Poisson's ratios for adjacent layers) is strictly only applicable to the case of transmission of a plane compressional wave across the boundary between two elastic media, with no slipping at the boundary. However, its application here appears justified in that heights determined from Eq. 19 agreed well with design thicknesses where these were available.

4. Using the radius of the block above and the experimentally determined mass, the height, h_n, of the nth block was found from

$$h_n = \frac{\left[0.956 \frac{M_3}{\rho} \tan\theta_n + r_n^3\right]^{1/3} - r_n}{\tan\theta_n} \qquad (20)$$

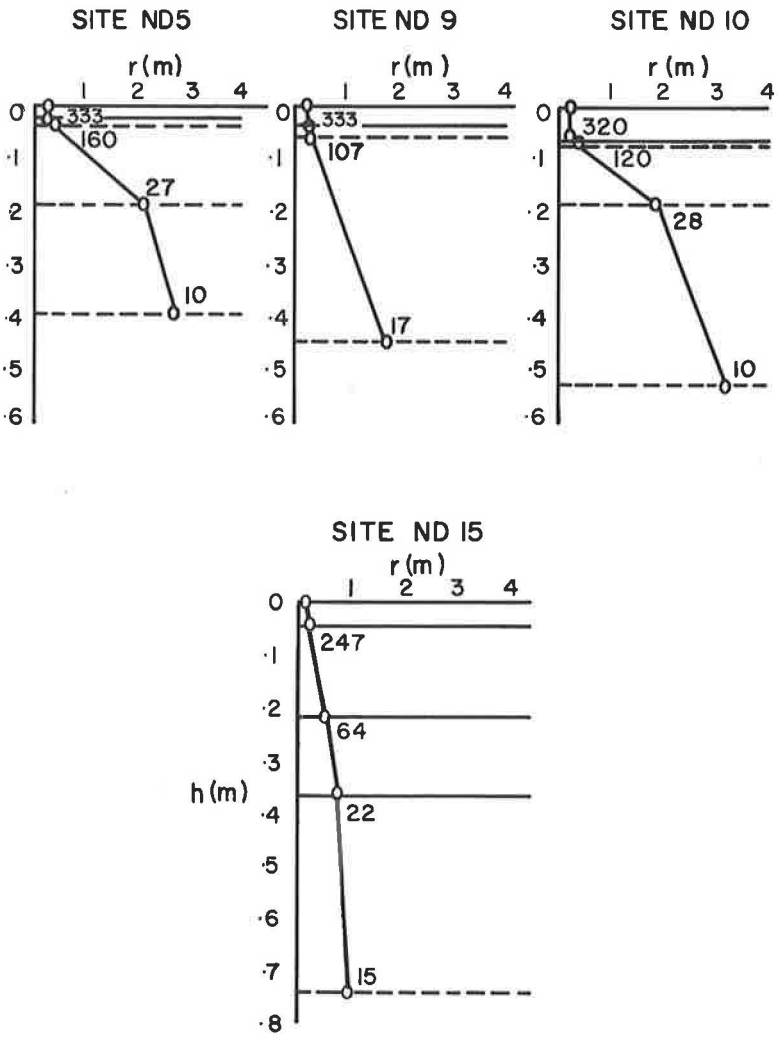

Figure 15. Variation of radii, r, with depth, h, for sites with unstabilized foundation.

and the radius of the base from

$$r_{n+1} = r_n + h_n \tan\theta_n \qquad (21)$$

In some cases it was found necessary to combine more than one mass layer as explained earlier. A useful guide is provided by noting the frequency above which a block ceases to vibrate. For similar types of construction these limiting frequencies should be of the same order of magnitude at a given level.

The calculated variations of radii, r, with depth, h, are given in Figures 15 to 17, where separation between design layers is indicated by full horizontal lines, whereas the dashed lines show levels obtained by the method described under 3 and 4. It will be noted that the differences are usually small, and in some cases the design and calculated layer levels are practically coincident.

The numbers given at the layer separation points in Figures 15 to 17 refer to the frequencies above which the layers of the construction, below these points, are not involved in the vibration. No satisfactory model was obtained for ND8 because of lack of realistic masses.

In general, it may be remarked that the models for the sites such as ND15 (no stabilization) and ND13 (lime stabilization in the base) extend to greater depth than the

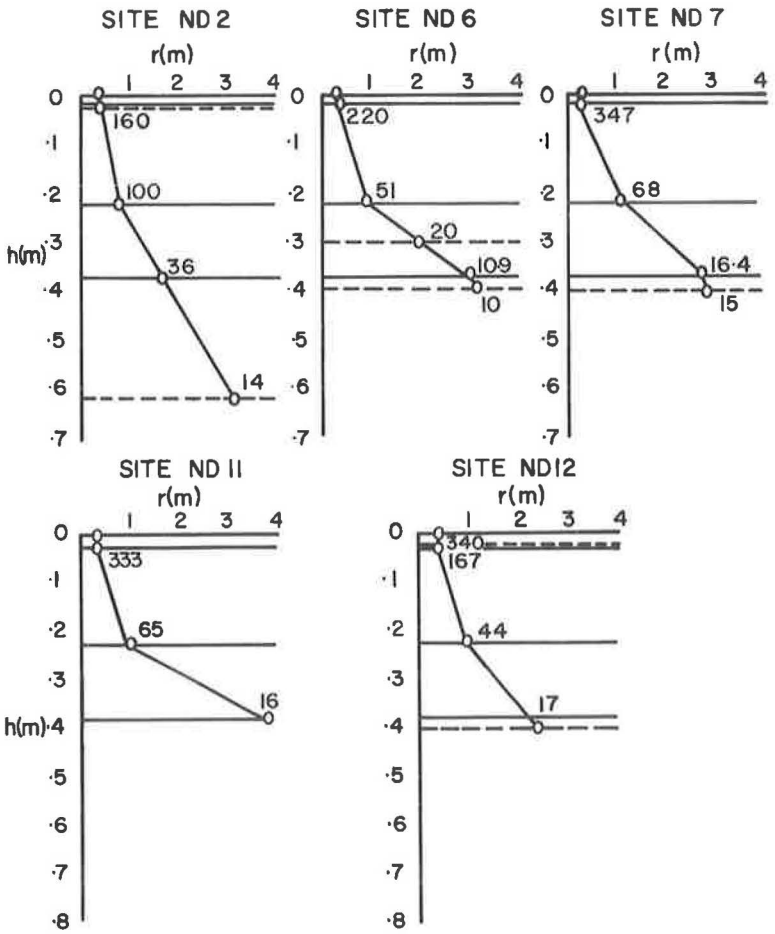

Figure 16. Variation of radii, r, with depth, h, for sites with stabilized subbase.

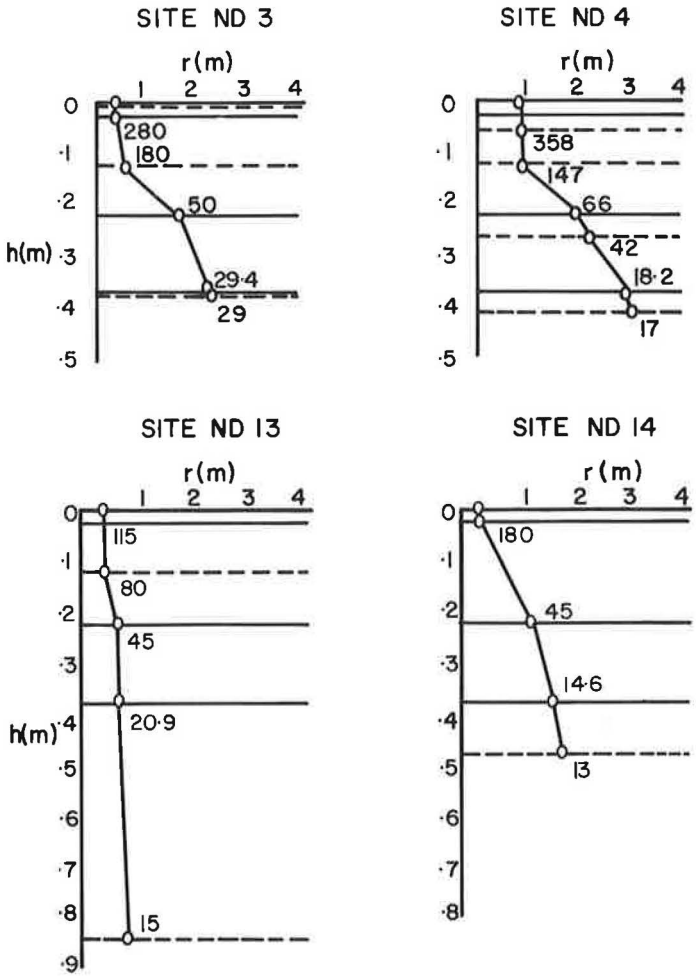

Figure 17. Variation of radii, r, with depth, h, for sites with stabilized subbase.

models for more solid constructions, such as ND3 and ND4 (with cement stabilization in the base). Furthermore, for most of the stabilized constructions (Figs. 14 and 15) (except for ND13), the model does not extend much below the subbase level, showing that forces at frequencies higher than 10 c/s do not affect the subgrade to any considerable extent.

ESTIMATION OF STIFFNESS AND RESISTANCE ASSOCIATED WITH EACH LAYER OF THE CONSTRUCTION

Stiffnesses and resistances obtained from impedance measurements (Tables 4 and 5) represent the total values of these quantities associated with that part of the model which is in a state of vibration at any particular frequency.

The mechanism of the model can be understood by reference to Figure 18, where it is shown how, for any layer, n, both stiffness, S_n, and resistance, R_n, have been divided into side components, S_{n1} and R_{n1}, and base components, S_{n2} and R_{n2} such that

$$\left.\begin{aligned} S_n &= S_{n1} + S_{n2} \\ R_n &= R_{n1} + R_{n2} \end{aligned}\right\} \quad \text{and} \qquad (22)$$

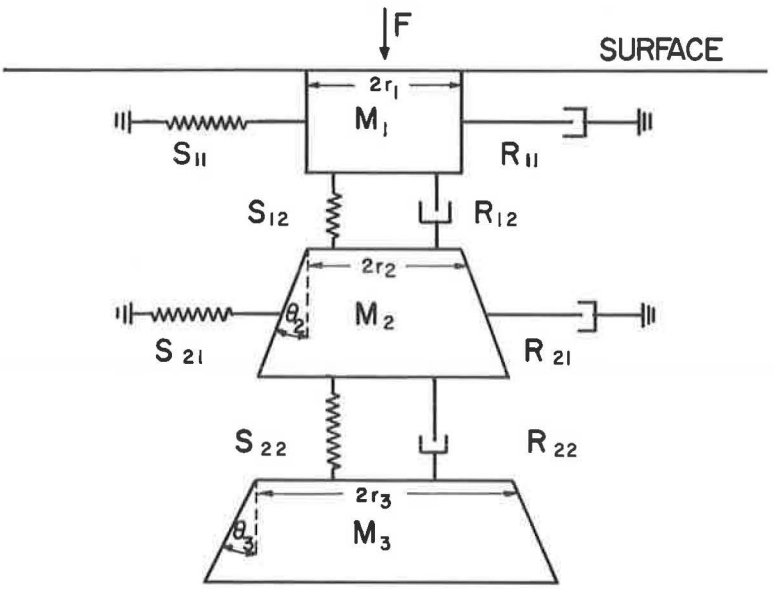

$$S_n = S_{n1} + S_{n2}$$
$$R_n = R_{n1} + R_{n2}$$

$$S = S_{11} + S_{21} + \text{-----} + S_n$$
$$R = R_{11} + R_{21} + \text{-----} + R_n$$

Figure 18. Diagram illustrating the division of stiffness, S, and resistance, R, into base and side components.

When, at a lower frequency, layer (n + 1) comes into action, it attaches itself rigidly to a layer n over the whole base area, so that S_{n2} and R_{n2} become inoperative, whereas S_{n1} and R_{n1} remain effective. Values of S_n and R_n may therefore be obtained for any particular layer from

$$\left.\begin{aligned} S &= S_{11} + S_{21} + \ldots\ldots + S_n \\ R &= R_{11} + R_{21} + \ldots\ldots + R_n \end{aligned}\right\} \qquad (23)$$

provided that values for the side components of higher layers are known. S and R are the experimentally measured values in the frequency range for which n layers are disturbed.

The problem resolves itself therefore into finding how S_n and R_n divide themselves into base and side components.

Inasmuch as the vibrating mass is considered rigid, stiffness and resistance effects are confined to the surface of the model. It is therefore assumed that frictional resistance and compressive stiffness are proportional to the surface area of the model.

Because the stiffness over the base is necessarily compressive, and the stiffness along the sides is partly compressive and partly tangential, this must be taken into account in the calculations.

If Poisson's ratio is assumed as $\mu = 0.5$ and s = compressional stiffness per unit area, then s/3 = shear stiffness per unit area. Consider an applied vertical force, F; then (Fig. 19).

The compressive component on slant face = F sin θ.

The tangential component on slant face = F cos θ.

The compressive stiffness = s sin θ perpendicular to surface.

The shear stiffness = s/3 cos θ parallel to surface.

The compressive stiffness along vertical = s $\sin^2\theta$.

The shear stiffness along vertical = s/3 $\cos^2\theta$.

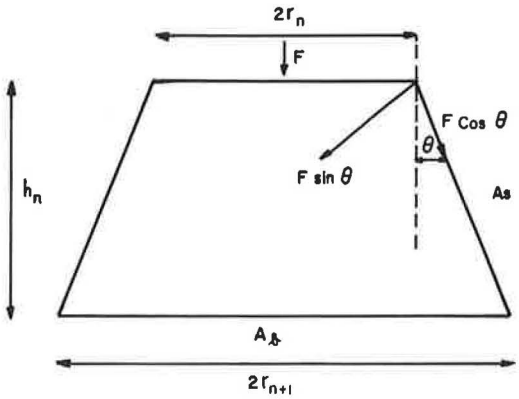

Figure 19. Determination of S_{n1} and S_{n2} from S_n.

Therefore, total vertical stiffness per unit area of curved surface is

$$s\,(\sin^2\theta + 1/3\cos^2\theta) =$$

$$s\,(1 - 2/3\cos^2\theta)$$

If A_s = area of curved surface and A_b = area of base,

the vertical stiffness due to the curved surface = $A_s\, s\,(1 - 2/3\cos^2\theta)$

and vertical stiffness due to base = $A_b s$

$$\frac{\text{side stiffness}}{\text{total stiffness}} = \frac{S_{n1}}{S_n} = \frac{A_s\,(1 - \frac{2}{3}\cos^2\theta)}{A_s + A_b\,(1 - \frac{2}{3}\cos^2\theta)} \tag{24}$$

The resistance per unit area will be independent of direction if the tangential friction is equal to perpendicular friction so that

$$\frac{R_{n1}}{R_n} = \frac{A_s}{A_s + A_b} \tag{25}$$

A_s and A_b are fully defined by the geometry of the model and, in terms of the notation of Figure 19, are given by

$$A_b = \pi r^2_{n+1} \tag{26}$$

$$A_s = \pi\,(r_n + r_{n+1})\sqrt{h_n^2 + (r_{n+1} - r_n)^2} \tag{27}$$

and for the case of a cylinder

$$A_s = 2\pi r_n h_n \tag{28}$$

The division of S_n and R_n into their components depends, therefore, essentially on the ratio A_s/A_b. Consequently, with the thickness, h_n, fixed, the error introduced by a slightly incorrect model is greatly reduced, because both A_b and A_s vary in the same direction with a change in r_{n+1}, and a slightly incorrect value of ρ does not affect significantly their ratio.

Some of the results representative of each group are given in Figure 20 for S_n and in Figure 21 for R_n. The horizontal axis is proportional to the depth below the surface, whereas the heights are proportional to either S_n or R_n. The heights of the shaded areas are proportional to the side components (S_{n1} and R_{n1}, respectively), and the heights of the unshaded areas are proportional to the base components (S_{n2} and R_{n2}, respectively).

No direct comparison is possible, as all the sites tested represent different constructions. However, some general trends and characteristics are evident, as follows:

1. In general the value of S_n decreases as n increases, irrespective of the type of construction. An exception occurs for site ND3, where the maximum value of S_n occurs in the base course, which is cement-stabilized.

2. The value of S_{n1} (shaded areas) varies in a manner depending on the construction. In particular, the value of S_{11} is always lower than S_{21}, indicating that, as soon as the frequency is sufficiently low to excite the base, the surfacing contributes very little to the overall stiffness of the construction.

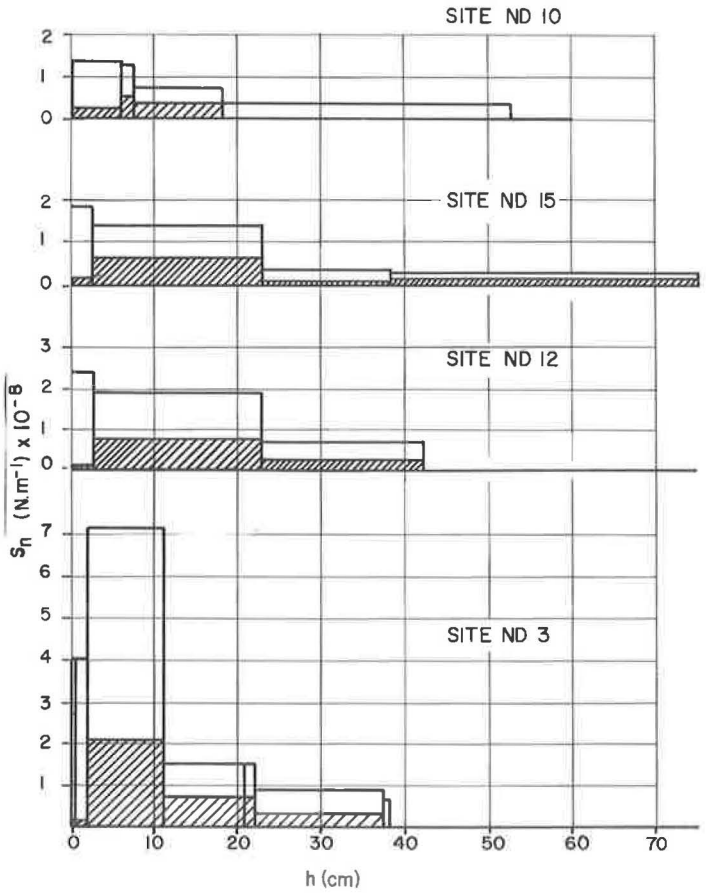

Figure 20. Comparison between S_n values for 4 types of constructions.

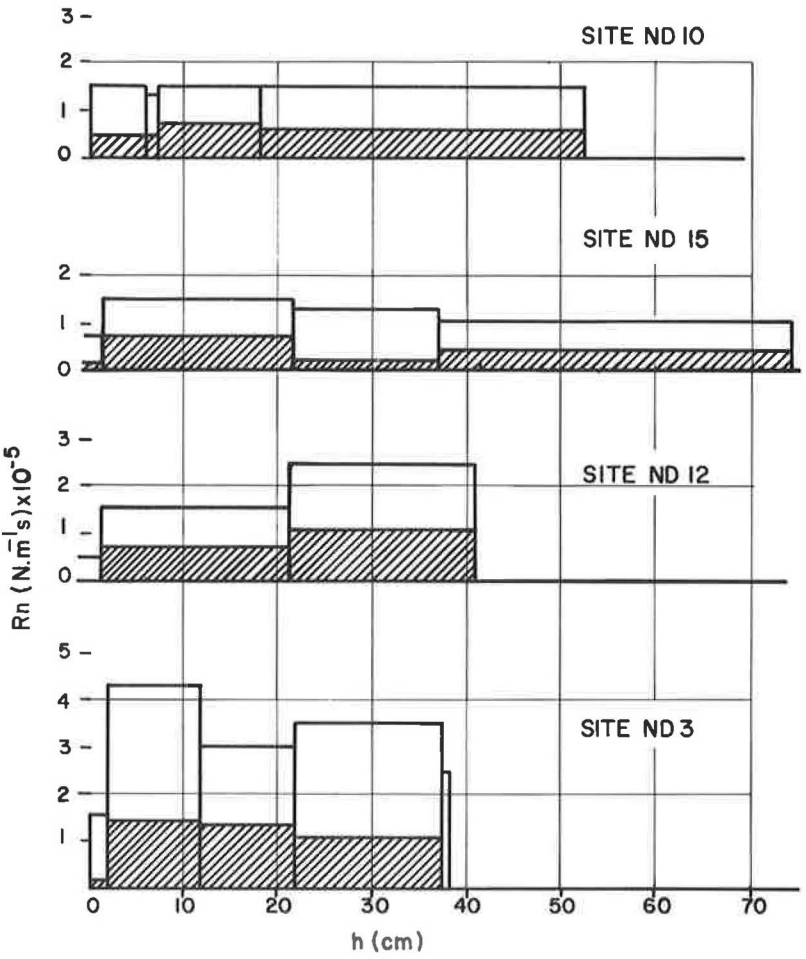

Figure 21. Comparison between R_n values for 4 types of constructions.

3. Large differences occur in the value S_1, S_2 and S_3 between the various constructions. The individual values cannot be taken as characteristic properties of the structure as a whole, but they represent the contribution of the layer under consideration to the overall stiffness of the construction.

4. Stiffnesses are higher for the better types of construction in Figure 20, corresponding stiffnesses being higher for the stabilized sites ND3 and ND12 than for the unstabilized sites ND10 and ND15.

Similar considerations are applicable to the R values given in Figure 21:

1. There is no definite trend in the R_n values, which vary to a much lesser extent with depth than do the S_n values.

2. The same is true of R_{n1} (shaded areas). Again R_{11} is always lower than R_{21}, indicating that the contribution of the surfacing to the overall resistance of the construction is negligible at lower frequencies.

3. Resistances are higher for the stabilized constructions (such as ND3 and ND12) than for the unstabilized ones (e.g., ND10 and ND15.)

DETERMINATION OF MECHANICAL QUANTITIES AT VARIOUS DEPTHS OF THE CONSTRUCTION

Once a suitable model has been found from impedance measurements and from it the division of S and R into their components for each layer estimated, other mechanical quantities at any depth of the construction may be estimated. The accuracy of such calculations will depend on the reliability of the original experimental data and on the degree of approximation involved in the various assumptions made in deriving the model which, it must be emphasized, is a simplification of actual conditions.

It is nevertheless felt that, if the same procedure is consistently followed in interpreting the measurements, comparison between results obtained from similar constructions should be relatively free of any errors introduced by the geometric dimensions of the model. In this and the following section, methods are developed for calculating the vertical stresses at any depth of the construction and the mean energy loss per cycle in a given layer at different frequencies of applied loading. Heukelom (4) has related frequency to equivalent vehicle speed, but this relationship has not been used here. It should be borne in mind that, although the values deduced here apply to sinusoidal loading, the passage of a vehicle wheel imposes a single impulse containing a large number of frequencies which are attenuated to different extents by the layers. The shape of such a surface impulse will therefore change with depth, whereas with sinusoidal loading, the amplitude only is reduced with depth, but not the shape.

Determination of Stresses

The adopted model consists of a rigid mass, M, vibrating with a vertical velocity, v, determined by the applied force, F, and mechanical impedance, Z, according to

$$v = \frac{F}{Z} \tag{29}$$

Therefore, with Z determined, v may be calculated for any impressed force, and the whole mass moves with this velocity.

The total force, F_n, acting at any level, h_n, of the construction over a horizontal area, A_n, will be

$$F_n = vZ_n \tag{30}$$

in which Z_n is the impedance of the model below level h_n. Z_n will be a function of frequency and in general is given by

$$Z_n = R' + j\left(\omega M' - \frac{S'}{\omega}\right) \tag{31}$$

in which R', M' and S' are the total values of R, M and S below the level, h_n, which are effective at the frequency $\omega/2\pi$. Because the model itself is a function of frequency it follows that, at a given level, Z_n is calculated by inserting the correct values of the primed parameters at the frequency under consideration.

The stress, σ, at level h_n and frequency f is then obtained from

$$\sigma = \frac{F_n}{A_n} \tag{32}$$

or

$$\sigma = \frac{vZ_n}{A_n} = \frac{F}{A}\,\frac{Z_n}{Z} \tag{33}$$

Inasmuch as both Z and Z_n are complex quantities, it follows that F_n and σ are not in phase with the applied force.

Stresses were calculated in this way for all the sites investigated at the levels of separation between layers. Because the area of cross-section of the cone increases with depth, the top of each cone section should in all probability give the value of maximum stress in the material.

The results for one of the representative sites are presented as curves of stress, σ, vs frequency at various depths in Figure 22. A wheel load of 1 ton (or 6.93×10^3 newton) was assumed, the load being spread evenly over a circular area of radius 10 cm (i.e., equal to the area used in the dynamic tests). This load corresponds to a surface stress of 2.20×10^5 N/m^2. Hence in all the graphs, σ has this value at all frequencies for h = 0.

The following points should be noted in Figure 22:

1. σ decreases rapidly as the depth h, necessitating the use of a logarithmic scale on the vertical axis.
2. At the higher frequencies (corresponding to higher vehicle speeds) only the higher layers are affected and hence the plot of σ for lower layers is very limited. This implies that, at high speeds, the surfacing and the base are of importance and subbase and subgrade are operative at low speeds only.

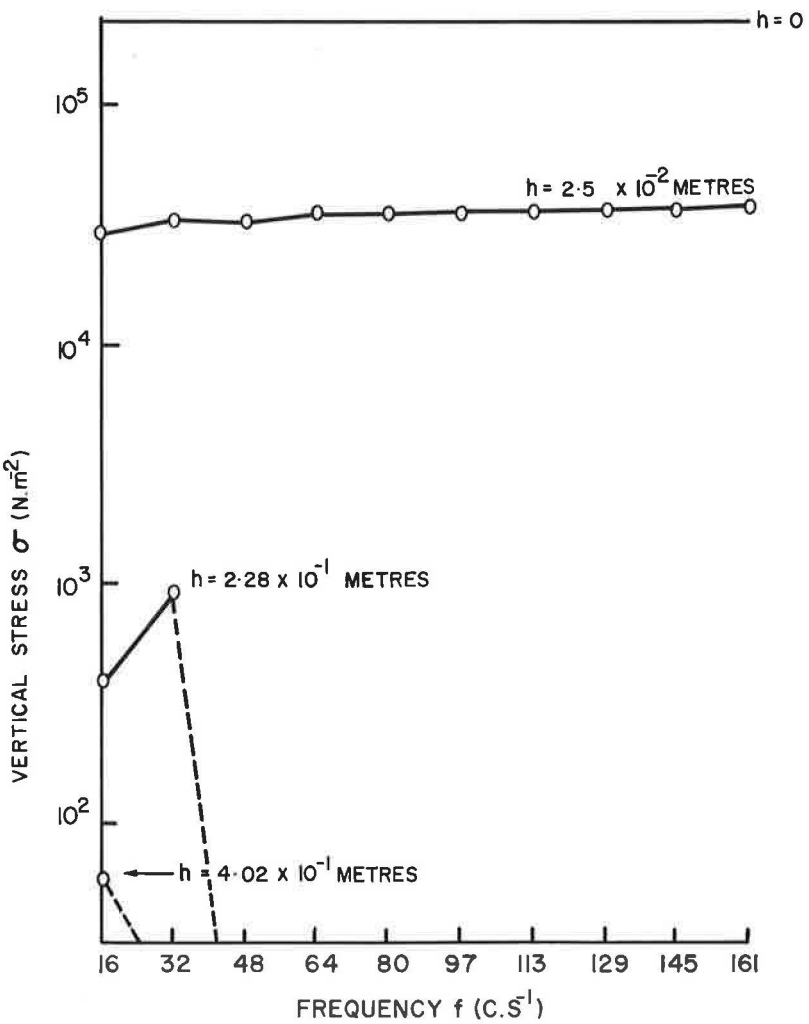

Figure 22. Variation of vertical stress, σ, with frequency, f, at various depths for site ND 12.

3. Graphs for the lower layers show a tendency to rise as f increases, showing that maximum stress occurs at the maximum frequency at which the layer is affected.

As σ varies comparatively little with frequency, its mean value may be used as an index of the reduction of stress with depth, independent of frequency. The results for some representative sites are shown in Figure 23, in which the heights of the lines are proportional to the logarithm of σ and their positions on the horizontal axis to the depth. The figures at the top of each line indicate the frequency below which the corresponding stresses exist.

The reduction of σ with depth is most marked for the sites with stabilized foundations (ND12 and ND3), but much less marked for ND15 where the foundation is unstabilized. The rapid drop in σ for site ND10 is remarkable and might be ascribed to the fact that the penetration macadam surfacing was apparently not well compacted.

Determination of Energy Loss

Another quantity which may be determined from the impedance method, after a geometrical model has been assumed, is the energy loss in unit volume. It is more

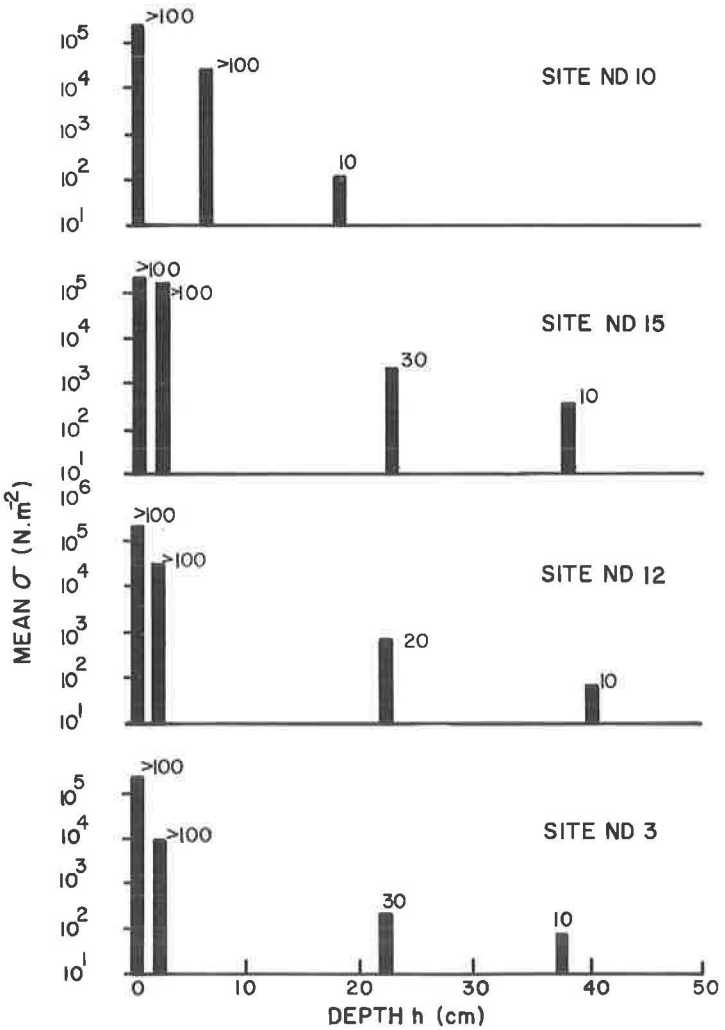

Figure 23. Mean vertical stress, σ, for 4 types of constructions at various depths.

useful to determine this quantity for one cycle, as in this form it may be more directly related to the passage of a single wheel load on the surface.

As before, it is assumed that the applied vertical force is sinusoidal and of frequency $f = \omega/2\pi$. Then the stress, σ_n, at a depth, h_n, below the surface will also be simple harmonic and of the form

$$\sigma_n = \sigma_o \exp(j\omega t) \tag{34}$$

and the vertical velocity, v (constant for the whole moving mass), is

$$v = \frac{F_n}{Z_n} = \frac{\sigma_n A_n}{Z_n} = \frac{\sigma_o A_n}{|Z_n|} \frac{\exp(j\omega t)}{\exp(j\theta_n)} \tag{35}$$

in which θ_n is the phase angle between σ_n and v, at depth h_n, i.e.,

$$\tan\theta_n = \frac{X_n}{R_n} \tag{36}$$

Hence

$$v = \frac{\sigma_o A_n}{|Z_n|} \cos(\omega t - \theta_n) \tag{37}$$

If p is the instantaneous power distributed throughout the vibrating volume, V_n, below h_n,

$$p = \vec{F}_n \vec{v} = A_n(\vec{\sigma}_n \vec{v}) = \frac{A_n^2 \sigma_o^2}{|Z_n|} \cos\omega t \cos(\omega t - \theta) \tag{38}$$

Thus the average power over volume below h_n is

$$\bar{p} = \frac{\int_0^T p\, dt}{T}$$

in which $T = 1/f$ = period of vibration.

Therefore, $\bar{p} = \frac{\omega}{2\pi} \frac{A_n^2 \sigma_n^2}{Z_n} \int_0^{\frac{2\pi}{\omega}} \cos\omega t \cos(\omega t - \theta_n)\, dt = \frac{A_n^2 \sigma_o^2}{2|Z_n|} \cos\theta_n$

Hence the energy lost per cycle in volume, V_n, below h_n is

$$E_n = \frac{A_n^2 \sigma_o^2}{2f|Z_n|} \cos\theta_n = \frac{A_n^2 \sigma_o^2}{f|Z_n|} \cos\theta_n$$

Expressing E_n in terms of v (see Eq. 33) gives

$$E_n = \frac{F_n\, v}{f} \cos \theta_n \tag{39}$$

If E_{n+1} is the energy lost per cycle in a vibrating volume, V_{n+1}, below some greater depth, h_{n+1}, and $E_n - E_{n+1}$ is the energy lost per cycle in the vibrating volume between depths h_n and h_{n+1},

$$E_n - E_{n+1} = \frac{v}{f}\left[F_n \cos \theta_n - F_{n+1} \cos \theta_{n+1}\right]$$

and finally, w, the energy lost per unit volume between levels h_n and h_{n+1} is

$$w = \frac{E_n - E_{n+1}}{V_n - V_{n+1}} = \frac{v}{f} \frac{F_n \cos \theta_n - F_{n+1} \cos \theta_{n+1}}{V_n - V_{n+1}} \tag{40}$$

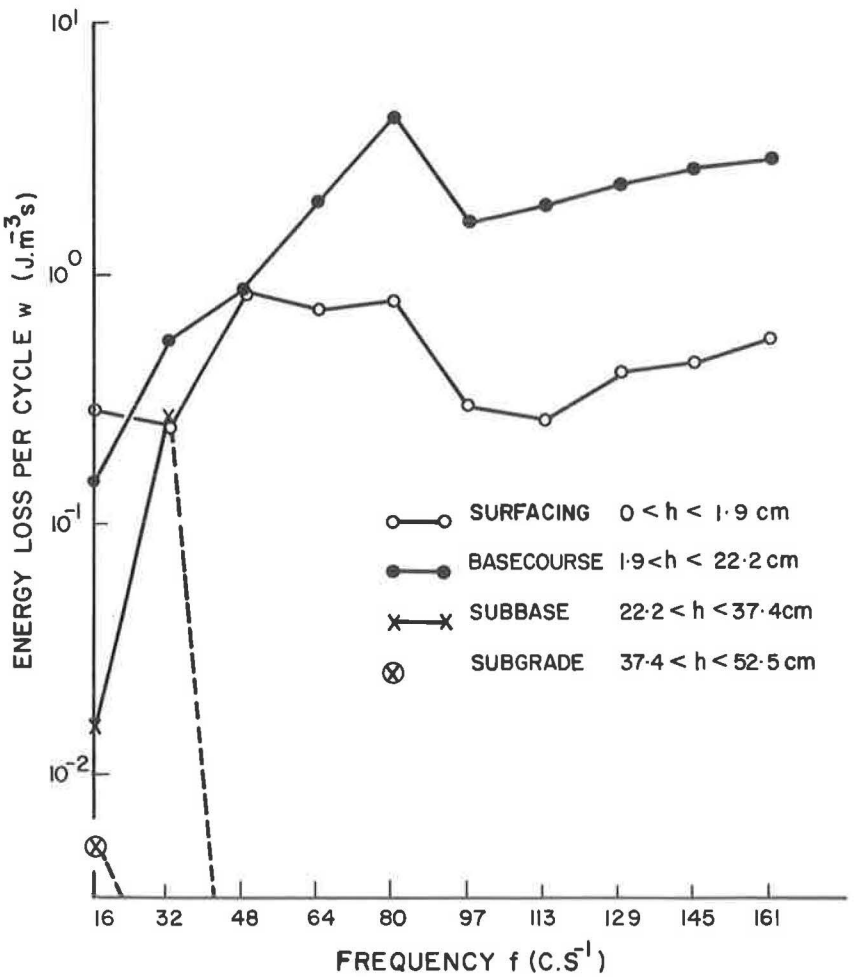

Figure 24. Variation of energy loss per unit volume per cycle, w, with frequency, f, for site ND 3.

in which the V's are calculated from the model's geometric dimensions.

Values of w at various levels obtained for site ND3 (as an example) are shown in Figure 24. In general, the graphs are characterized by a rising curve which reaches a maximum just before the layer under consideration becomes inoperative. Apart from the maximum, the energy loss is lower for deeper layers, but the latter show also a steeper gradient. The general characteristics shown in Figure 24 occurred also in the graphs for the other sites.

DISCUSSION

A method has been outlined by which a number of the mechanical properties of a layered construction can be determined quantitatively, almost entirely from impedance measurements.

No claim is made that the geometrical model adopted is unique or the most suitable, nor that further improvement in the method of determining its geometric dimensions cannot be made. However, the facts that the model must be symmetrical in a horizontal plane and that static theory indicates that the load spreads over a wider area with increase in depth, point unmistakably in the direction of a conical shape. There is a need for a more exact method of determining the radii of the cone frustums and this possibility is being investigated.

In spite of the uncertainty existing over the actual dimensions of the model, the general equations and methods of deduction of the more practical quantities (such as σ and w) should remain correct. Numerical values for the stresses are perhaps less reliable than those for the energy loss, in that the former are directly dependent on the square of the linear dimensions of the model, whereas the latter depend only on the volume (i.e., is independent of the radii of the cones).

Further vibration measurements on other roads are being carried out, as the 14 different types of construction tested are insufficient to enable conclusions of a general nature to be drawn; variations are, however, in the expected direction in most cases. A large number of measurements of nominally equivalent constructions are required to give more definite indication of the validity of the assumptions. Independent measurements of the derived quantities (e.g., the introduction of strain gages at various depths of a road construction, as is being done by Dempwolff, et al (7)), would be of great value, and are being planned.

The present work will be recognized as having its origin in the work of Baum (8). Progress, however, has been made in that it has been possible to assign values of the parameters to each layer of the construction. The remainder of the work follows almost axiomatically. An essential part of this development has been the wider frequency range of the equipment which has provided a more complete picture of mechanical behavior and without which no progress could have been made.

The present method of treatment can be criticized on the grounds that the problem has been oversimplified. The purpose, however, has been to attempt to bring impedance measurements one step nearer to the stage where they can become useful tools in the hands of the road engineer. The following applications can at present be envisaged:

1. Study of the deterioration of any road construction under traffic, by repeated measurements at regular intervals.
2. Survey and assessment of existing roads, and localization of required improvements.
3. Control of construction during road-building operations to check that each layer falls within required tolerances.
4. A simplification of rational design, based on elastic theory.

ACKNOWLEDGMENTS

The authors wish to thank C. H. Freeme and J. van Blerk who carried out the work in the field and Mrs. Y van Niekerk who assisted with the lengthy numerical computations.

REFERENCES

1. Heukelom, W., "Dynamic Stiffness of Soils and Pavements." Proc., Symp. Vibr. Test. Roads and Runways, Amsterdam (April 1959).
2. Hueter, T. F., and Bolt, R. H., "Sonics." Ch. II, 9-18, Wiley (1960).
3. Lorenz, H., "Vibration Testing of Soils." Proc., Symp. Vibr. Test. Roads and Runways, Amsterdam, 111 (1959).
4. Heukelom, W., "Analysis of Dynamic Deflexions of Soils and Pavements." Géotechnique, 11: 224-243 (1961).
5. Baum, G., "Bericht uber dynamische Untersuchungen an der Versuchsstrecke Grunbach dausgefuhrt in den Jahren 1957 bis 1961." Report presented at meeting of "Unterbau" of Forschungsgesellschaft fur den Strassenwesen, Konstanz (July 1962).
6. Jones, R., "Surface Wave Technique for Measuring the Elastic Properties and Thickness of Roads—Theoretical Development." Brit. J. Appl. Phys., 13: 21-29, London (1962).
7. Dempwolff, R., Ewers, J., and Morell, G., "Messung von Verformungen in Asphaltbefestigungen unter Rottender Last." Strasse und Autobahn, 11: 391-395 (1961).
8. Baum, G., "Dynamische Untersuchungan an Strassen." Strasse und Autobahn, 8: 277-282 (Sept. 1959).

Discussion

E. N. THROWER, British Road Research Laboratory, Harmondsworth, England. — This paper presents a purely empirical discussion of the interpretation of dynamic stiffness tests on road constructions. It is based on a collection of arbitrary assumptions and ad hoc arguments which are difficult to discuss in a coherent fashion. Picking out just a few points:

1. It would have been somewhat less confusing if the results quoted by the authors for the impedance of a site had conformed to the definition given under "Principle of Impedance Method," where it is defined as the ratio between the total force exerted on the pavement itself, and its velocity. It is implied in the section on "Description of Experimental Sites and Data," however, that the results quoted refer to the ratio between the force applied to the vibrator foot and the pavement velocity; to obtain the impedance as originally defined the quoted values of ωX must be corrected by subtracting the reactance ωMg of the foot.

2. The arguments presented under "More Complete Interpretation of Experimental Data" assertion that the "mass" parameter will vary as f^{-3} does not involve the layered character of the construction. In fact, if true at all, it is true in particular for a semi-infinite uniform material. The calculations made by Sung (9), however, show that, on the contrary, ωX varies parabolically with frequency over the relevant part of the frequency range, so that the "effective mass" is constant. Thus there is no foundation for this argument. Further, if the argument were valid at all, it should be valid at all frequencies. Why then, is the dependence of the mass term (as distinct from the total ωX) taken as applying only at low frequencies? Lastly, the argument assumes that the phase velocity of the waves concerned is independent of frequency. Which of the many modes of vibration of a layered structure do the authors have in mind?

3. The assertion, implicit in "Description of Experimental Sites and Data," that M_e can never be negative, is also untrue; indeed, Figure 4 shows that at this site, $-\omega X$ increases with frequency, up to about 100 c/s, and this implies a negative value of M_e, as deduced from the plot of ωX against ω^2 used by the authors. This situation is avoided in the report by switching to an f^{-1} plot, but similar effects can also occur in the higher frequency range. Thus, if a sufficient degree of acoustic mismatch occurs between two adjacent

layers a resonant condition can arise from the reflection of longitudinal or shear waves at the interface. The resulting fluctuations in ωX cause negative values of M_e. Similar effects can arise from reflection of flexural waves at the edges of a road. Both these phenomena have frequently been observed in experiments made at the British Road Research Laboratory.

4. In connection with these points, perhaps the authors would indicate how their analysis would apply to the curves of Figure 25, which are calculated from the theoretical results of Warburton (10) and refer to the similar case of an elastic layer (shear modulus G, Poisson's ratio $\frac{1}{4}$) of thickness H, loaded over a circular region of radius r_0, and superimposed on an infinitely rigid substratum. The model thus assumes an infinite mismatch between the two media, and is to that extent unrealistic. Nevertheless, some sites approach this limiting case fairly closely, and the main effect of the finite mismatch (and of damping inherent in the materials) will only be to reduce the height of the resonant peaks. (The dotted portion of the curves denotes regions where the fluctuations in ωX are so rapid that the curves are not known accurately.)

5. Use of Eq. 19 which gives the angle of refraction of a plane longitudinal wave at the interface between two media, to calculate the angle of the fictitious cones of the author's model is without justification. Arbitrary introduction of this equation from the theory of an elastic continuum into a field to which it is completely irrelevant is unwarranted.

6. Although the elastic properties of bituminous materials vary rapidly with temperature, no reference is made to the effects of this parameter on the impedance values.

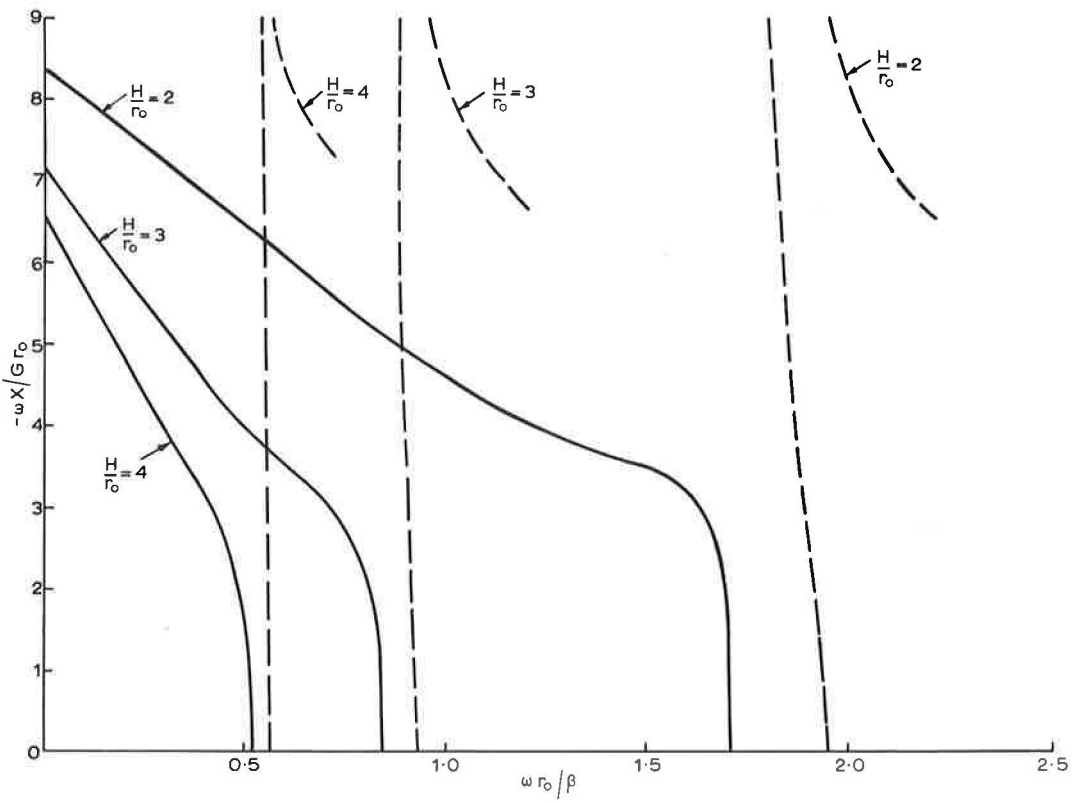

Figure 25. Dynamic stiffness of an elastic layer on a rigid subbase; after Warburton (10).

In general, analysis of impedance data along the lines of this paper, in which analysis and discussion of the real phenomena visible in the test results (e.g., thickness resonances, etc.) are replaced by the arbitrary introduction of as many ad hoc hypotheses as seem necessary, can ever lead to any fruitful results, especially when, as here, the hypotheses are unsupported, and indeed, often contradicted, by the available theoretical results.

References

9. Sung, T.Y., ASTM Special Publication No. 156.
10. Warburton, G.B., Jour. Appl. Mech., Paper No. 56-A-35.

R. JONES, British Road Research Laboratory, Harmondsworth, England. —A few comments are offered here on the ambiguities and misconceptions which seem to exist in the section on "Wave Propagation Tests."

The writer's theory to which the authors refer is based on the assumption that the road may be treated as a plate (or composite plate) on liquid layers. These assumptions have allowed an interpretation of the experimental data obtained at the higher test frequencies, usually in the range of about 700 to 24,000 c/s, on major road constructions in Great Britain. The analysis permits the elastic moduli and thicknesses to be calculated of those cement- or bituminous-bound layers which have a considerably higher shear modulus of elasticity than the underlying soil or unbound granular layers. It is unfortunate that the apparatus described by the authors is not able to operate in that part of the frequency range in which alone a rational interpretation is believed to be possible at this time.

Absence of an adequate theory to interpret the low-frequency data does not, however, deter the authors from making confident identification of the depth and shear properties of the layers of a road by a process which has no rational justification. In data relating velocity to wave length obtained on our experimental roads we have been able to identify certain velocities which were constant over a range of low frequencies (long wave lengths) with the shear wave velocities in underlying granular materials. However, this inference was made only when the elastic properties of the granular layer had been previously measured during the road construction. As the authors are possibly aware, the depth of bases and subbases inferred from these results by the rule given in the paper (i.e., depth equals one-third of a wave length) was up to 7 times the true depth (11). Moreover, the depth found by the author's third rule can actually change with the date of test because the relations between wave length and velocity on a bituminous road change with the road temperature and, therefore, this causes changes in the complex modulus of elasticity of the bituminous materials. In the present state of knowledge, it is doubted that any region of constant velocity can be identified with the shear wave velocity of a particular layer without prior information. Why should not similar effects occur at compressional wave velocities, or even at velocities completely unconnected with the characteristic velocities in any of the layers as was found recently (12) in theoretical work on an earth model?

It is to be regretted that the authors have included so many apparently dubious assumptions and have, moreover, expressed confidence in their deductions without offering adequate proof or confirmation by means of independent measurements. This method of presenting controversial ideas is particularly regrettable because it can mislead newcomers to the subject and perhaps delay the development of a rational interpretation of the experimental data.

References

11. Jones, R., "Interpretation of Surface Wave Propagation: Data on Road Constructions, at Low Frequencies." Dept. of Scient. and Indus. Res., Road Res. Lab. Res. Note No. RN/3830/RJ.
12. Harkrider, D.J., Hales, A.L., and Press, F., "On Detecting Soft Layers in the Mantle with Rayleigh Waves." Bull. Seis. Soc. A., 53:3, 539-548 (Apr. 1963).

M. E. SZENDREI and S. H. KÜHN, Closure—The authors wish to thank Dr. Jones and Mr. Thrower for their comments, which emphasize the present difference between two possible approaches in the investigation of dynamic testing. Although a number of theories have been developed, mostly based on idealized assumptions, little correlation has been established with practical road behavior. A number of other investigators, both in Europe and in the U.S.A., have on the other hand already applied dynamic tests, using approximate theories, with success in road and airfield design and the evaluation of performance under traffic.

In following the latter approach the authors admit that some of the assumptions made can be criticized theoretically. However, in the absence of an applicable theory and the evidence that results with practical significance are obtained, it is at present considered to be the best approach to investigate this promising method. The mechanical model used in the derivation of stresses and energy losses does not necessarily represent the only or best possible solution to the observed data. This fact has been mentioned in the introduction as well as at various stages in the text.

In reply to the comments by Mr. Thrower, the following are offered:

1. The fundamental definition of mechanical impedance, Z, defined as the complex ratio of applied force to resultant velocity, has been strictly adhered to throughout the text. Naturally it has been applied in each case with due regard to the mechanical model under consideration. Thus, all the experimental ωX values include the mass Mg of the vibrator foot, which under experimental conditions is an integral part of the vibrating system. When, however, in the latter part of the text, the net impedances of the construction are considered, Mg has been subtracted from the total mass measured.

2. The variation of the mass, Me, as f^{-3} at low frequencies is an experimental fact determined on different types of construction. Sung's theory, applying to a semi-infinite medium and assuming zero damping, therefore does not apply to the test conditions described. No theoretical explanation can be offered as to why the mass Me at high frequencies is constant, but this again follows from experimental results. The three-parameter model assumes a rigid mass in which the velocity is very high compared to the velocity in the surrounding medium.

3. The assumptions in regard to the variation of m with frequency have been consistently applied for all constructions analyzed and no cases were found where Me varies as f^{-3} in the high-frequency range. The authors feel that a negative Me is practically meaningless and that it is consequently justified to modify the assumed model to satisfy this condition at low frequencies. The authors do not agree that the experimentally determined decrease in ωX at low frequencies is due to acoustic mismatch, because this fact has been established on all the constructions tested, which included a variety of boundary conditions.

4. The suggested method of analysis could not be applied to the curves of Figure 25 drawn from the theoretical results of Warburton, inasmuch as curves of this shape have not been found to occur at the sites tested so far.

5. The application of Eq. 19 to the problem under discussion is admittedly of doubtful validity. It has been used only in extreme cases for the lower layers, when there was no independent means of determining the depth of the cone. However, as a check, it was applied also to a number of cases where the heights were known from the design profiles, and the resulting agreement was good as shown by the dashed lines of sites ND 6, ND 7 and ND 12 in Figure 16.

In reply to the comments by Dr. Jones, the following are offered:

The apparatus used in the wave propagation tests could operate satisfactorily up to a few kc/s. Higher frequencies, however, were not required to calculate the thickness of the surfacing-base combination, because it was determined entirely from the intersection of the first and second branches of the dispersion curves. The data required for the determination of λ were therefore the lower frequency points on the first branch and the higher frequency points of the second branch. The thickness of the surfacing was obtained from the design profile.

The other objection raised is the use of the empirical determination of depth assumed equal to one-third the wave length. Further work on this aspect since writing the paper has confirmed that approximate depths can be determined by the $\lambda/3$ rule:—

1. A number of wave propagation tests carried out on roads with a cement-stabilized base and compacted subbase (of 3 times the base thickness) were analyzed using Jones' theory and the $\lambda/3$ method. It was interesting to find that the differences in measured base thickness obtained by the two methods differed by no more than 5 percent.
2. Wave propagation tests were repeated on a road during various stages of construction. As each layer was added, the phase velocity/wave length dispersion curves were displaced along the wave length axis by an amount equal to about three times the thickness of the additional top layer.

According to a private communication received from the U.S.A., a theoretical derivation of layer depths using the wave length and the ratio of phase velocities in adjacent layers gave values varying between $\lambda/2$ and $\lambda/3$ and correlated well with independent direct measurements.